Available online at www.eccomasproceedia.org
Eccomas Proceedia COMPDYN (2023) 4693-4705

ECCOMAS
Proceedia

COMPDYN 2023
9th ECCOMAS Thematic Conference on
Computational Methods in Structural Dynamics and Earthquake Engineering
M. Papadrakakis, M. Fragiadakis (eds.)
Athens, Greece, 12-14 June 2023

DAMPING ASSESSMENT OF BRIDGES FOR PERFORMANCE BASE DESIGN

Juan M. Mayoral[1] **and Mauricio Pérez**[1]

[1] Institute of Engineering, Universidad Nacional Autonoma de Mexico, Mexico City, Mexico

e-mail JMayoralV@iingen.unam.mx

Abstract

Modern performance bridge design relies on reaching controlled stages of damage and failure modes to ensure both safety and economy. In high seismic zones, the design philosophy should be based on the ability of a bridge to deform inelastically and ductilely, allowing some damage to fused elements to decrease the potential internal forces during earthquakes. This approach, however, requires a careful determination of the potential damping expected to occur on the structure and foundation. In the case of single-span or two-span bridges, the abutments have a significant impact on the bridge's performance, mainly in the longitudinal vibration modes, so the determination of the damping in the abutment is critical. In most reference bridge design manuals, the recommended damping values for abutments usually range from 5% to 10%, which results in a more robust design of the structure due to the limited allowance of energy dissipation.

In particular, this paper presents a numerical study of the energy dissipation available in the abutments of common bridge typologies. The observed damage patterns in bridges near the epicentral zone induced by recent subduction earthquakes in Mexico were analyzed using 3D finite difference models. To simulate the development of damping in the abutment, a fully non-linear approach was adopted, where the hysteretic model Sig3 coupled with the Mohr-Coulomb constitutive model was considered for the mechanical and dynamic behaviour. From the results gathered in here, the relationship between damping and abutment displacements was established, and it is clearly demonstrated that the inclusion of large damping values during bridge design can lead to both cost-efficient and safe designs if a good abutment deformation assessment is conducted.

Keywords: Damping assessment, seismic design, bridge abutments, numerical modelling.

ISSN:2623-3347
Peer-review under responsibility of the organizing committee of COMPDYN 2023.
doi: 10.7712/120123.10751.20861

1 INTRODUCTION

In recent years, it has been proven that the nonlinear stress-strain behaviour of the backfill soil in the abutments has a significant impact on the seismic performance of bridges. When they are skewed with limited spans, the abutments become more important because they absorb a considerable portion of seismic forces, mainly in the longitudinal direction [1-3].

Nevertheless, dynamic equilibrium between inertial forces and, restoring and damping forces is commonly assessed using simplified methods based on beam-spring models, in which the interaction with soil is commonly simulated with linear springs and viscous dashpots. In case of the two last ones, due to soil nonlinearity, such characteristics can vary widely during strong ground motion, modifying the predicted internal forces of the structural elements of the bridge. So, when the abutments have a significant impact on the bridge's performance, it is critical to utilize appropriate stiffness and damping values based on the expected strains or adopt a fully nonlinear approach capable of reproducing the hysteretic behaviour of the soil. For example, when there isn't available data of damping values, the LRFD Seismic Analysis and Design of Bridges Manual [4] suggest a maximum damping ratio of 10% for the longitudinal vibration modes in the case of single-span or two-span bridges with abutments and 5% in the case of longer concrete bridges. However, this approach requires a detailed assessment of the potential damping expected to occur on the structure and foundation, which must be agreed upon with the level of shear strain in the soil because it can experiment yielding during the seismic loads and reach large damping values.

When an extreme event occurs, the performance bridge can be directly assessed by observing and identifying the induced principal damage patterns, and determining whether the design prediction agrees with the observed behaviour. As a result of this evaluation, a back analysis can be made by reproducing the observed performance using appropriate analysis models capable of simulating the structure's conditions. Likewise, it can possible inferred the shear strain levels that the soil reach during the ground shaking as well as the damping developed.

This paper focuses on the assessment of bridge damage caused by the Mw 7.7 September 19, 2022, Michoacán earthquake near the epicentre. In summary, despite the high peak ground acceleration values reached in the visited zone, which nearly reached 1 g according to site seismic stations, good performance was observed [5]. According to the damage observed, abutments were the most affected elements, allowing for quick remedial actions and the avoidance of serviceability loss. This evidence suggests that during the ground shaking, these elements were able to dissipate a large amount of energy, reducing the seismic demand on the bridge's structural elements.

To achieve this, 3D finite difference models were developed with the software FLAC^{3D}, where common bridge damaged typologies of the zone were simulated. In summary, two-span and three-span bridges were such with affected abutments, so both of thus were considered in the analysis. The considered input motion, corresponds to the time story recorded by the COMA station, located in rock 40 km away from the studied site, during the mentioned earthquake. With the developed models, the observed damage is reproduced in terms of displacement and plastic zones in the soil backfill, where the hysteretic model Sig3 coupled with the Mohr-Coulomb constitutive model were considered to simulate the mechanical and dynamic behaviour. With the results gathered in here, it was possible to infer the damping values reached during the earthquake, observing that values higher than 10% are available in the abutments.

2 OBSERVED DAMAGE FOLLOWING THE 2022 MICHOACAN, MEXICO, EARTHQUAKE

On September 19, 2022, an earthquake with a moment magnitude of M7.7 struck the central region of Michoacan near Coalcoman in Mexico. The massive amount of energy released was caused by a reverse faulting mechanism with a hypocenter 15 kilometers deep at 18.22 north latitude and -103.29 west longitude [6]. This location corresponds with the so-called Middle America Trench, where the Cocos plate is subducting beneath the North American plate. Along this active megathrust plate boundary, there have been numerous M>7 earthquakes in the last 50 years, including the M8.0 Michoacan/Mexico City earthquake of 1985 and the followed large M7.6 aftershock 32 hrs. after (See Figure 1a).

The spatial distribution of the root mean square (RMS) of the horizontal (north-south and east-west components) peak ground accelerations (PGA) obtained from hard-rock recordings is shown in Figure 1b. The map depicts the potential extent of potentially damaging shaking caused by the 2022 earthquake (i.e., light, moderate, and severe). The Coalcoman earthquake produced moderate to high magnitudes in the epicentral region. The highest RMS PGA was recorded at station MMIG, about 8 km from the epicentre, with 902 cm/s², followed by station COMA, about 132 km from the epicentre, with 206 cm/s² [6].

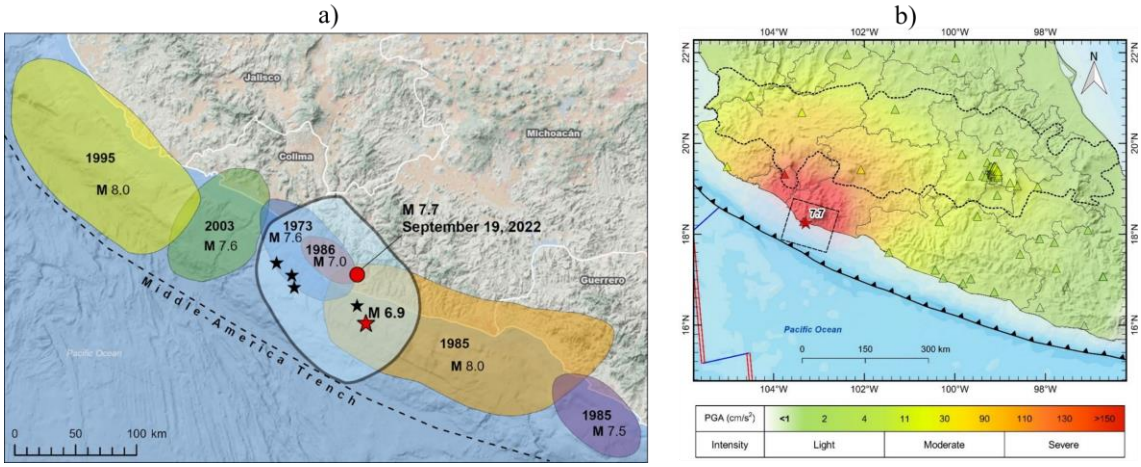

Figure 1: a) Approximate location of subduction zone rupture planes, west-central Mexico, since 1973 [5] b) Map of peak ground acceleration [6].

As can be seen, the seismic event caused significant ground shaking and damage, primarily in the coastal states of Colima and Michoacan, with PGA of up to 1g in the epicentral area. According to the observations made during virtual and visual reconnaissance, the principal affectations along the main and secondary roads of the zone consisted of slides of cutting slopes, lateral and longitudinal cracking of pavement, and damage in the elements of bridges. Regarding the last point, the observed damage was mostly related to the opening of joints in the decks of the bridges (the typical gap of joints was about 6 to 10 cm wide), vertical cracking in abutments, lateral displacements of decks, and cracks in shear keys of pier caps. All the damaged bridges were in operation, and only the bridges located in El Ticuiz, Michoacan, and Colima City, Colima, were undergoing repair work that was initiated after the earthquake [5].

Figure 2: Common bridge damage after the September 19th, 2022, Michoacan Earthquake, in the coastal area of Colima and Michoacan [5].

Figure 2 shows some pictures of the most common damage patterns exhibited by the bridges in the visited zone near the epicentre. As can be seen, the injured elements suffer plastic deformation primarily in the abutments and in the lateral shear keys of the pier caps; on the other hand, the substructure behaved elastically in all cases. Those damage patterns exposed the design philosophy followed in high seismic zones, in which the ability of a bridge to deform inelastically and ductilely is a necessity, due to the inelastic response having both economic and technical bases. In terms of economics, it is rational to allow some damage rather than divert unnecessary resources toward an extreme event with a low probability of occurrence. Technically, it is reasonable to design some elements as fused structures, which limit the internal forces. With this approach it reduces the structure's vulnerability to earthquakes larger than the design event [7].

3 REGIONAL GEOLOGY AND VS_{30} ESTIMATION

Following the identification of the damaged bridges, the regional geology in the damaged areas was investigated to determine whether any amplification of the movement was due to site effects. According to the survey areas, almost all the damaged bridges were in the coastal zone, where the topography was moderately flat, implying the presence of unconsolidated materials beneath the most damaged areas.

The following descriptions correspond to the coastal region of Colima, and Michoacan states. Such coastal region is distinguished by the predominance of recent poorly consolidated materials such as polymictic conglomerate and Pleistocene sandstones (QptCgp-Ar), as well as Holocene alluvium, residual soils, and fine sands (Qal). Similarly, there is an alternation between intrusive igneous rocks, primarily granite and granodiorite (KsGr-Gd), and igneous pyroclastic materials such as andesitic tuffs and breccias composed of subangular andesite fragments welded in a sand-clayey matrix (Kapa-A, Kap-BvA, and KapceTa-Ar). Figure 3 depicts the distribution of the dominant geological units in the aforementioned coastal area [5]. The surveyed roads with damaged bridges are also shown, as are the seismic stations where the highest values of PGA were recorded.

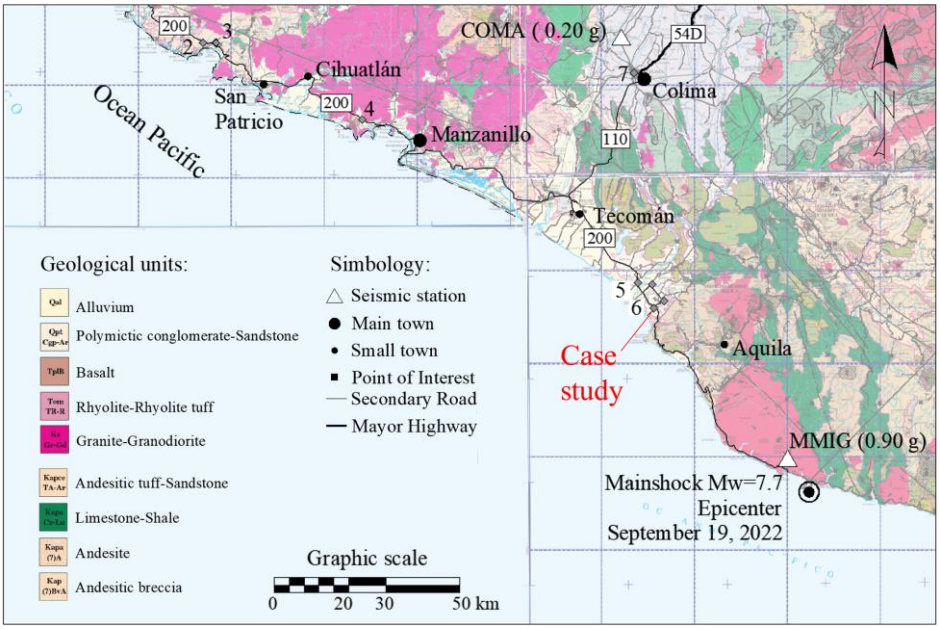

Figure 3: Geological map of the coast areas with bridge damage [5].

Given the lack of Vs data for sites, there were applied proxy models for Vs30 prediction that were developed for California. The procedure involved looking up site surface geology, relating the mapped geology to geologic categories used in California [8], and then assigning the California-based mean μlnV and standard deviation σlnV values. The geology used in this process corresponds to the map shown in Figure 3. According to Ahdi et al. [9], using a proxy relationship developed in one region and applied in another without local validation is a reasonable approach as long as the estimation includes epistemic uncertainty.

Figure 4a shows the histogram of the collected Vs30 data in California from downhole, cross hole, and suspension log surveys for young alluvium materials with moderate flat surface slopes. Given a LogNormal distribution, the range of Vs values in the first 30 m is defined as 240 to 365 m/s. In addition, Vs profiles presented by Tonatiuh Dominguez et al. [10] for the region of Manzanillo in similar geological conditions were considered. Figure 4b depicts the Vs profile developed based on the Vs30 estimation, the S1 and S3 profiles corresponding to Manzanillo, and the idealized profile considering all three profiles; as can be seen, the variation was small. This last one, was the Vs profile used to simulate the conditions experienced by bridges damaged during the earthquake.

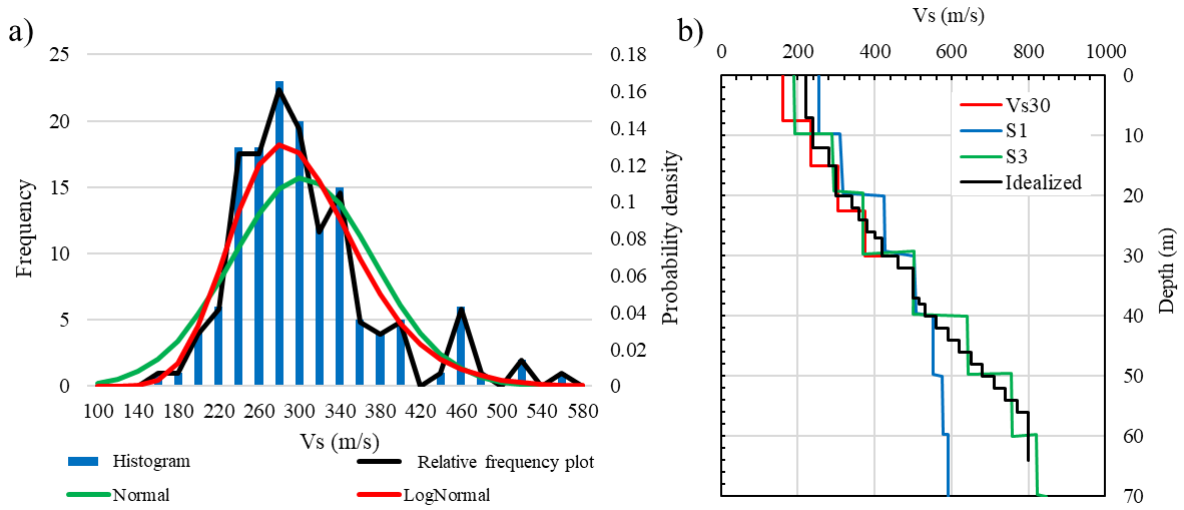

Figure 4: Histogram of Vs30 values obtained in alluvium soil on moderately flat areas from California (modified from [10] b) Estimation of Vs profile for the site under study.

4 CASE STUDY

According to the observed common topologies at the visited zone, it was defined a representative three-span bridge as a case of study. Figure 5 describes the structure elements that conform the bridge as well as their dimensions. In summary the superstructure consists of a non-continuous upper deck resting on five support AASHTO I-beams separated every 2.85 m, which are structurally tied. Such beams are simply supported by the pier caps and the abutments. The middle supports are composed by concrete pier caps with shear keys on the sides to restrict the lateral seismic movements, likewise this is supported by four concrete columns of Ø=0.8 m, separated every 4.0 m, which are joined monolithically; regarding to its foundation the same diameter of the columns corresponds to the piles of 8.0 m length which are tied monolithically to the columns with a pile cap of 2.0 m width and 0.8 height. The abutments of the bridge are comprised by a concrete cantilever retaining wall where the support beams lean, at the sides there have wing walls which are used to retain the backfill soil, which were considered as a compacted silty sand. In addition, an earth slope in front of the retaining wall was considered as scour protection.

The location of the bridge was supposed in the coastal area of Michoacan, between the points 5 and 6 in the Figure 3, 70 km away from the epicenter. Corresponding to the mentioned regional geology, it was supposed a homogeneous layer of alluvium soil comprised of fine sand of medium compactness.

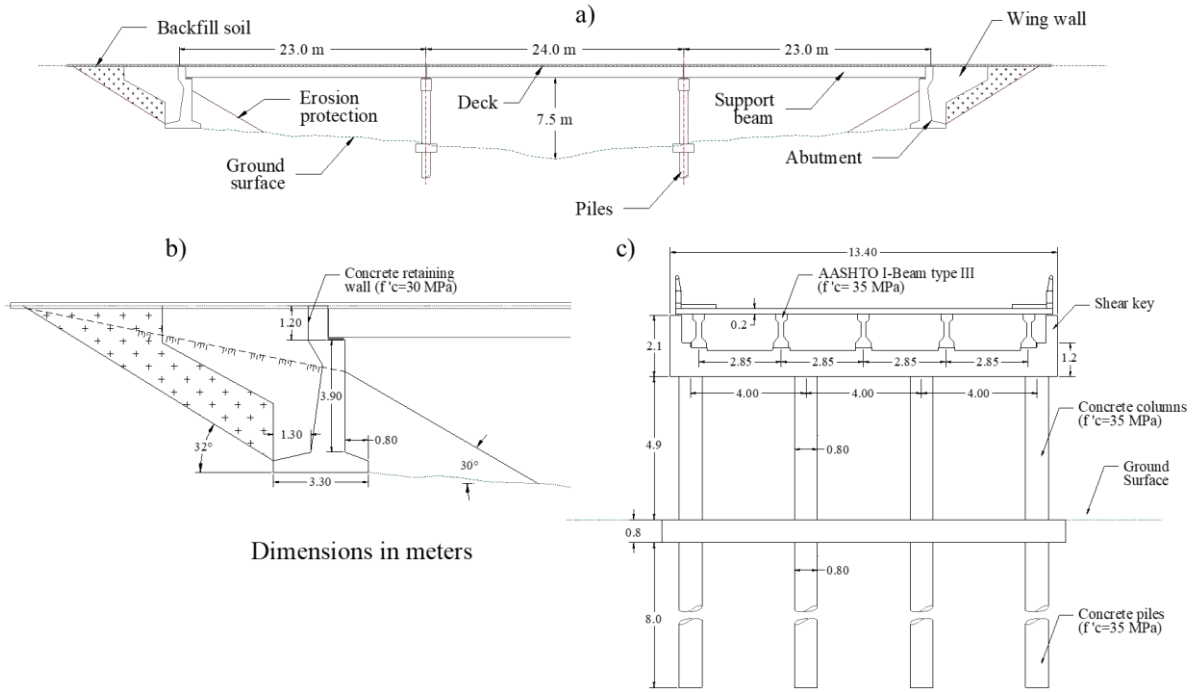

Figure 5: a) Longitudinal view of the bridge under study b) Abutment configuration c) Cross-section of the middle support and foundation.

4.1 Input ground motion

The dynamic response of the bridge was computed for the September 19th, 2022, Michoacan Earthquake, taking into account both the soil deposit and the soil-structure system. The strong ground motion recorded at station COMA (located in rock) was used as input time history in the dynamic analyses. Although the study site is located closer to the epicenter, similar seismic intensity was presented in the zone according to Figure 1b, therefore such record was considered reasonable to apply in the analyses. Figure 6 shows the measured accelerations for both orthogonal components, and their corresponding response spectra. Both components of motion were considered in the seismic response analyses.

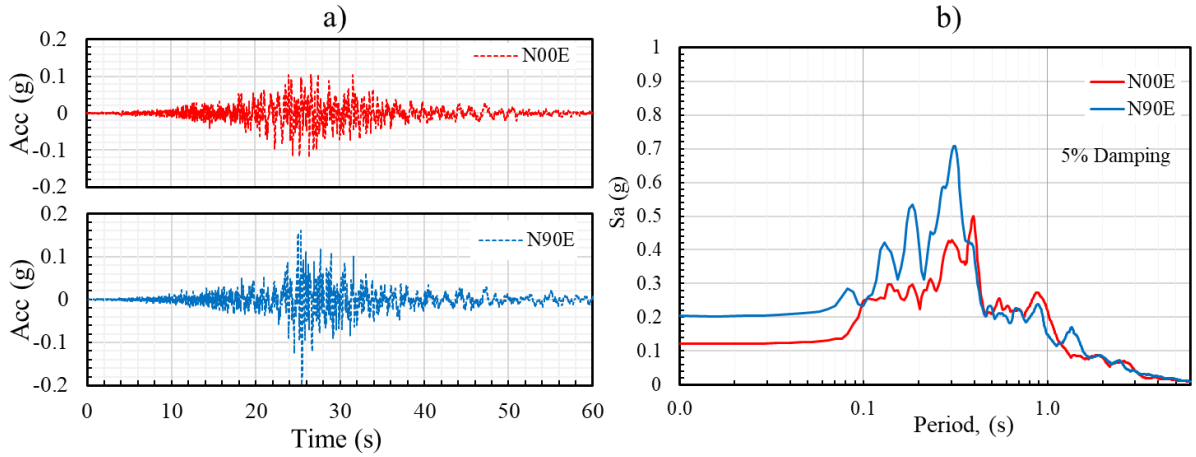

Figure 6: a) Time histories recorded in the COMA station during the September 19th, 2022, Michoacan Earthquake b) Response spectra of the time histories.

5 NUMERICAL MODEL

To simulate the strong ground motion caused by the September 19, 2020, Michoacan earthquake, in the studied area, a three-dimensional model was performed with the program FLAC^{3D}. Such model, consider the underneath soil, the backfill soil, and the structure elements of the bridge. Figure 7a depicts the global domain of the finite difference mesh, and Figure7b the structural elements of the bridge.

To represent soil behaviour, it was deemed appropriate to consider a Mohr-Coulomb failure criterion, due to the lack of information to define the soil parameters of more complex constitutive models. The geotechnical parameters considered are those shown in Table 1, the distribution of soil foundation was considered homogenous in the whole model and the backfill soil and earth slope protection according to Figure 5.

The model consists of 180960 three-dimensional elements representing the soil mass and the concrete retaining walls of the abutments. Within the domain of the model, further refinement of the mesh was adopted on the zones in contact with the structure. Also, several control points were located in these areas to monitor the interaction effects during the simulation, and at the edges and corners of the model to establish the free field seismic motion. Figure 14 shows the finite difference mesh considered in the simulation and the boundary conditions. To represent the structural elements of the bridge, BEAM elements were used to simulate the support beams, columns and pier caps, PILE elements to simulate the piles, and SHELL elements to simulate the deck of each span. The behaviour of such elements was considered elastic. The structural parameters considered are those shown in Table 2.

Table 1. Mechanical parameters of the solid elements.

Layer	$\boldsymbol{\gamma}$ (kN/m³)	**c** (kPa)	φ (°)	$\boldsymbol{E_{50}}$ (MPa)	$\boldsymbol{\nu}$
Alluvium	17.0	20	30	80	0.35
Backfill	18.2	51.20	30	140	0.28
Scour protection	17.0	15.60	27	110	0.34

Where γ is the unit weigh; **c** is the cohesion; φ is the friction angle, $\boldsymbol{E_{50}}$ is the secant elasticity modulus, and **ν** is the Poisson's ratio.

Table 2. Mechanical and geometrical parameters of the structural elements.

Bridge element	$\boldsymbol{\gamma}$ (kN/m³)	H / D (m)	A (m^2)	Ix (m^4)	Iy (m^4)	f'_c (MPa)	$\boldsymbol{E_s}$ (MPa)	**ν**
Support beam	24	1.15	0.35	5.2E-2	3.5E-3	35	2.64E+4	0.25
Columns and piles	24	0.80	0.50	2.0E-2	2.0E-2	35	2.64E+4	0.25
Pier caps	24	1.20	0.96	1.2E-1	5.1E-2	35	2.64E+4	0.25
Deck	24	0.20	-	-	-	30	2.52E+4	0.25

Where H is the height of the element; D is the diameter of the element; A is the cross-sectional area of the element; I_x and I_y are the moments of inertia about the transverse and longitudinal axis of the element, respectively; f'_c is the nominal compression resistance of the concrete; and *Es* is the Young's modulus of the element.

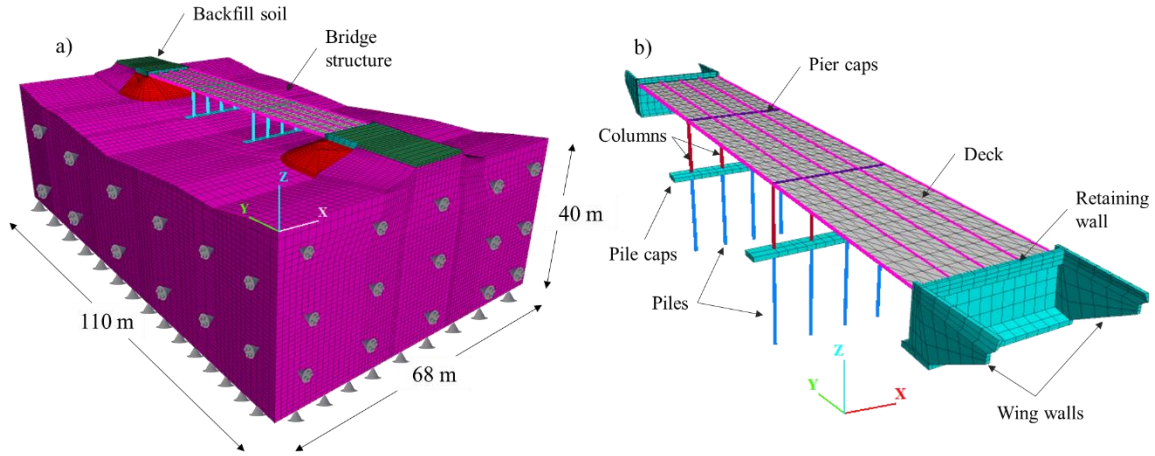

Figure 7: a) 3D numerical model used by the soil-structure interaction analysis b) Structural elements of the simulated bridge.

6 THREE-DIMENSIONAL SOIL-STRUCTURE INTERACTION ANALYSIS

Prior to the soil-structure interaction analysis, the input motion to apply at the base of the model was defined by the deconvolution of the surface ground motion with the program SHAKE [11]. To avoid wave reflections during the dynamic simulation and the allowance of radiation damping, quiet boundary conditions were defined at the model's base using Lysmer & Kuhlemeyer [12] formulation. In the case of the lateral faces of the model, Free field boundaries were considered using the formulation available in FLAC^{3D}.

Due to the lack of information from undisturbed samples of the site to define the non-linear behaviour of the alluvium soil, the upper and lower bounds proposed by Seed and Idriss [13] for normalized modulus degradation and damping, were deemed appropriate to use in the analysis. The curves proposed by Alhassan and VandenBerge [14] for backfill soil were also implemented. In the case of the concrete structures, a constant value of damping equals to 5% was used in the analyses.

The hysteretic model Sig3, which is available in FLAC^{3D}, was used to simulate the stiffness degradation and increase in damping of the soil during ground shaking according to the mentioned curves. Figure 8 depicts the curves defined for each layer, as well as the corresponding expected theoretical curves defined by the type of soil. Therefore, in summary, the aforementioned curves and the Mohr-Coulomb failure criterion characterized the mechanical behaviour of the soil. The bridge construction process was simulated prior to the dynamic analyses in order to establish static equilibrium and the initial conditions of stresses in both the soil and the structural elements.

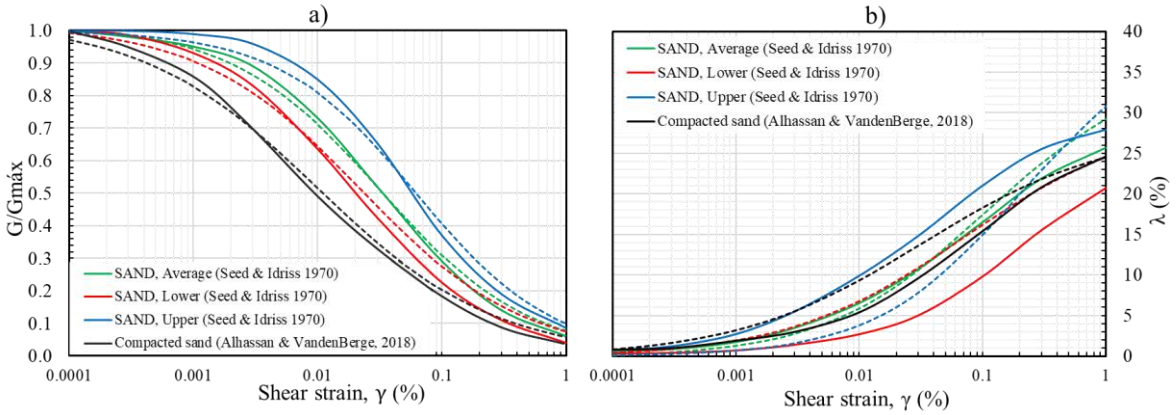

Figure 8: a) Normalized modulus degradation and b) Damping curves.

6.1 Results and discussion

The simulation of the strong ground motion caused by the September 19, 2022, Michoacan earthquake, in the coastal area of such state, was performed from the three-dimensional model (Figure 6). In summary the calculated surface and structure response of the simulated bridge, matched quite well with those observed in the visited damaged zones.

First, Figure 8a shows the results gathered from frequency domain and time domain analyses conducted with SHAKE and FLAC^{3D}, respectively, assuming one-dimensional SH waves propagating vertically. Also, the response spectrum of the input motion at the base of the model is shown, to observe the amplification caused by the soil column. Good agreement can be shown in the computed response obtained in the analysed case.

To observe the amplification from the foundation to the deck of the bridge, transfer functions were calculated in each direction as the ratio of the Fourier spectra of the deck between the Fourier spectra of the foundation, the obtained results are shown in Figure 8b. In comparison, the amplification is bigger in the transverse direction, reaching values of amplitude up to seven, while in the longitudinal direction the values are smaller than two. These big differences can be associated to the stiffness and damping developed in each direction. In the case of the transverse motion, there are eight columns and a constant damping of 5% due to the influence of the abutments is practically nil, so the stiffness is bigger, and the behaviour is almost linear which results in very little energy dissipation. On the other hand, the longitudinal motion is influenced to greater degree by the presence of the abutments which has nonlinear behaviour, and its stiffness can be degraded, which allows major energy dissipation.

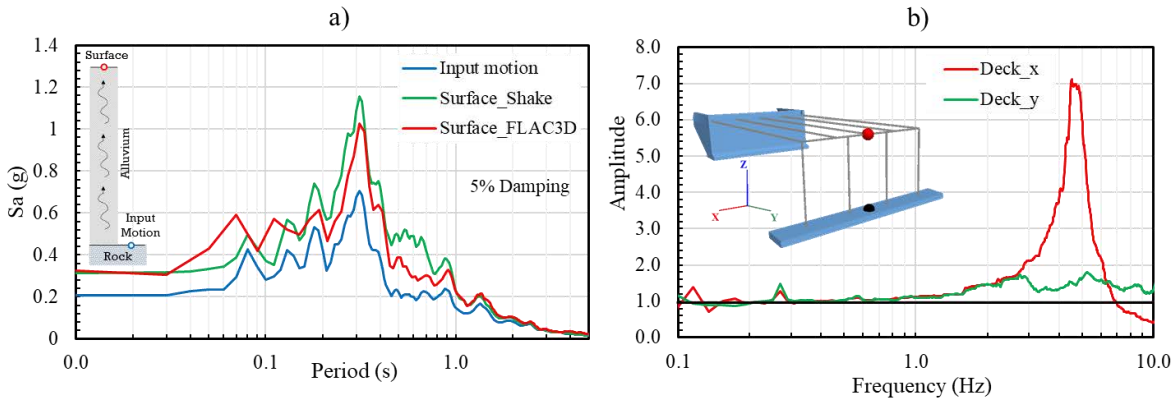

Figure 9: a) Response spectra at model´s surface b) Transfer functions between the foundation and the deck of the bridge.

The stress-strength ratio (SSR) was calculated at the end of the simulation to obtain a more detailed understanding of the abutment backfill soil. The SSR is a local indicator of the stress state's proximity to yield and is defined by the ratio between the deviatoric stress at the failure and the deviatoric stress developed in the simulation, which can be expressed as:

$$SSR = \frac{(\sigma_1 - \sigma_3)f}{(\sigma_1 - \sigma_3)} \quad (1)$$

$$(\sigma_1 - \sigma_3)_f = \frac{2c\cos\varphi + 2\sigma_3 \sin\varphi}{1 - \sin\varphi} \quad (2)$$

where c and φ are the cohesion and friction angle values from the Mohr-Coulomb failure criteria; σ_1 and σ_3 are the major and minor principal stresses, respectively, and the subindex f denotes failure. Values of $SSR \approx 1.0$ represent that the soil has reached the yielding stage, and the developed deviatoric stresses can induce cracking, instability, or excessive deformations.

Figure 10 depicts the SSR plot contours of one side of the bridge. Taken a simplified approach, the red zones can be associated to some potential mechanism of failure depending on its location. For example, the red zones at the toe of the slope can be interpreted as a sliding movement, and those in the crest of the embankment as settlement, protrusion, or lateral cracking. According to this interpretation, the zones with SSR ≈ 1.0 in the model, match well with the observed damage patterns after the earthquake in some bridges, such as those shown in Figure 3. Regarding to the backfill soil, it can be seen that it reached the yielding condition, so it can anticipate that high damping values were developed by the abutments.

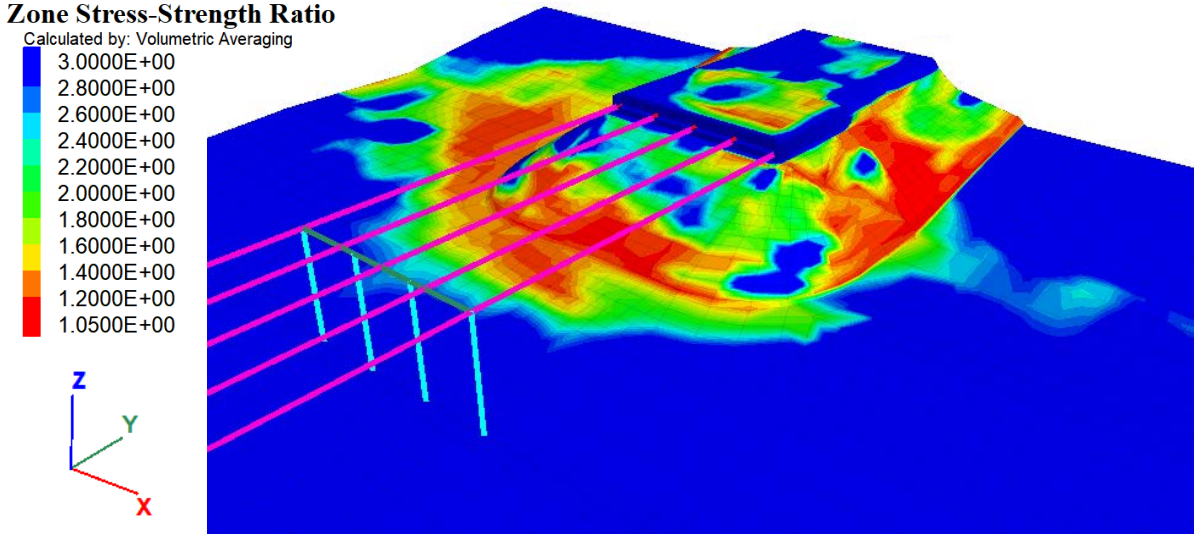

Figure 10: Plot contours of stress-strength ratio from numerical model in at the end the simulation.

To observe the stiffness degradation and the damping variation in the backfill soil, control points were located behind the retaining wall, in which G/Gmax and damping values were stored during the simulation. Figure 11a depicts the location of the control points and Figure 11b shows the obtained stored values by each control point during the simulation. As expected, the abutments developed high damping values up to 25 % in some cases, much more than the recommended value of 10%. However, it is worth defining the conditions experienced by the backfill soil according to the acceleration magnitudes of the time history. When comparing such time history with the values of Figure 11b, it can be noticed that after approximately 25 s (the instant of maximum acceleration), some points continue to grow even as the movement decreases. This phenomenon can be associated to the yielding or the failure of the element which causes the accumulation of plastic strains, allowing more energy dissipation.

So, following these results it is necessary to define that such high damping values are due to the yielding of the backfill soil. Nevertheless, before such instant of break point, it was possible to reach damping values up to 15%, which is still higher than the recommended maximum value.

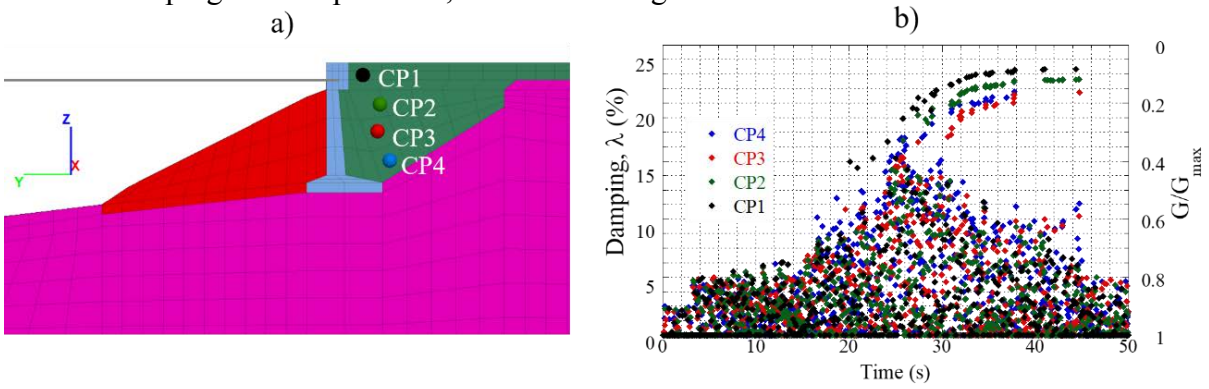

Figure 11: a) Response spectra at model´s surface b) Stored damping and G/Gmax values during simulation.

7 CONCLUSIONS

The energy dissipation available in the abutments of common bridge typologies in seismically active areas was assessed. In general, two mechanisms influence energy dissipation during seismic loading: material damping caused by nonlinear hysteretic soil behaviour and radiation, or geometric damping caused by energy dissipation through the half space. According to the developed analyses, it was observed that the abutment can develop damping values up to 15% before yielding and up to 25% after the backfill soil reach the failure, only because of the nonlinear hysteretic behaviour. This energy dissipation it was reflected on the amplification of the seismic motion on the deck of the bridge, particularly in the longitudinal direction where the maximum amplitude of the Transfer function was less than two. On the other hand, the seismic motion in the structure grows up to seven times on the transverse direction due to the influence of the abutment is almost nil, and the energy dissipation was minimal.

According to the results from the 3D numerical model, and the observed damaged patterns after the September 19th, 2022, Michoacan Earthquake, the optimal seismic bridge design is achieved by controlling the damage and failure modes in the bridge elements. This in turn implicates the correct estimation of the yielding point of fused elements, in order to allow some damage on it, giving to the bridge the ability to deform inelastically and ductilely. Likewise, this depends on the correct estimation of the potential damping in the abutments, mainly in the longitudinal vibration modes and in short two to three-span bridges, where its influence is critical.

In conclusion, with the allowance of large damping values during bridge design it is possible to achieve both cost efficiency and safety if a good abutment behaviour assessment is conducted.

REFERENCES

[1] A. Shamsabadi and M. Kapuskar, 'Nonlinear soil-abutment-foundation- Structure interaction analysis of skewed bridges subjected to near-field ground motions', Transp Res Rec, no. 2202, pp. 192–205, Jan. 2010, doi: 10.3141/2202-23.

[2] A. Shamsabadi and K.M. Rollins, 'Three-dimensional nonlinear continuum seismic soil-structure interaction analysis of skewed bridge abutments', Numerical Methods in Geotechnical Engineering, vol. 1, pp. 933–938, 2014.

[3] Y. Zhang, J. P. Conte, Z. Yang, A. Elgamal, J. Bielak, and G. Acero, 'Two-dimensional nonlinear earthquake response analysis of a bridge-foundation-ground system', Earthquake Spectra, vol. 24, no. 2, pp. 343–386, 2008, doi: 10.1193/1.2923925.

[4] M. L. Marsh, I. G. Buckle, and E. Kavazanjian Jr, 'LRFD seismic analysis and design of bridges: Reference manual', 2014.

[5] K. B. Clahan, D. A. de La Rosa, J. M. Mayoral V, M. D. Perez, and J. P. Stewart, 'GEOLOGICAL AND GEOTECHNICAL ENGINEERING RECONNAISSANCE OF THE SEPTEMBER 19, 2022, MICHOACAN EARTHQUAKE, MEXICO', 2022. doi: 10.18118/G6B95P.

[6] L. Ramírez-Guzmán, M. Jaimes, J. M. Mayoral, J. Aguirre, G. Ayala, M. L. Suárez, M. Contreras, D. de la Rosa, M. Alacaráz, E. F. Salazar, M. A. Macías and M. Ayala, 'The September 19th, 2022, M7.7 Coalcoman Earthquake', II-UNAM, Mexico, City, 2022.

[7] J. M. Mayoral, A. Badillo, and M. Alcaraz, 'Vulnerability and recovery time evaluation of an enhanced urban overpass foundation', Soil Dynamics and Earthquake Engineering, vol. 100, no. May, pp. 1–15, Sep. 2017, doi: 10.1016/j.soildyn.2017.05.023.

[8] C. J. Wills, C. I. Gutierrez, F. G. Perez, and D. M. Branum, 'A next generation Vs30 map for California based on geology and topography', Bulletin of the Seismological Society of America, vol. 105, no. 6, pp. 3083–3091, Dec. 2015, doi: 10.1785/0120150105.

[9] S. K. Ahdi et al., 'Site parameters applied in NGA-Sub database', Earthquake Spectra, vol. 38, no. 1, pp. 494–520, Feb. 2022, doi: 10.1177/87552930211043536.

[10] R. Tonatiuh Dominguez et al., 'Site response in a representative region of Manzanillo, Colima, Mexico, and a comparison between spectra from real records and spectra from normative', Soil Dynamics and Earthquake Engineering, vol. 93, pp. 113–120, Feb. 2017, doi: 10.1016/j.soildyn.2016.11.013.

[11] P. B. Schnabel, J. Lysmer, and H. B. Seed, 'SHAKE: a computer program for earthquake response analysis of horizontally layered sites, software'. 1972.

[12] J. Lysmer and R. L. Kuhlemeyer, 'Finite dynamic model for infinite media', Journal of the engineering mechanics division, vol. 95, no. 4, pp. 859–877, 1969.

[13] H. Bolton Seed and I. M. Idriss, 'Soil moduli and damping factors for dynamic response analyses', Berkeley, California, 1970.

[14] M. M. Alhassan and D. R. VandenBerge, 'Shear modulus and damping relationships for dynamic analysis of compacted backfill soils', Innovative Infrastructure Solutions, vol. 3, no. 1, p. 43, Dec. 2018, doi: 10.1007/s41062-018-0152-5